LA-UR-01-4401

*Approved for public release;*
*distribution is unlimited.*

| | |
|---|---|
| *Title:* | Modern Electron Accelerators for Radiography |
| *Author(s):* | Carl Ekdahl |
| *Submitted to:* | IEEE Transactions on Plasma Science |



**Los Alamos**
NATIONAL LABORATORY

# MODERN ELECTRON ACCELERATORS FOR RADIOGRAPHY

**Carl Ekdahl**

*Los Alamos National Laboratory, Los Alamos, NM, USA*

*Abstract*

Over the past dozen years or so there have been significant advances in electron accelerators designed specifically for radiography of hydrodynamic experiments. Accelerator technology has evolved to accommodate the radiographers' continuing quest for multiple images in time and space. Improvements in electron beam quality have resulted in smaller radiographic spot sizes for better resolution, while higher radiation dose now provides improved penetration of large, dense objects. Inductive isolation and acceleration techniques have played a key role in these advances.

## I. INTRODUCTION

The development of electron accelerators for radiography at many laboratories around the world has been motivated by a need for high-resolution data from hydrodynamic experiments driven by high explosives. Some of the largest hydrodynamic experiments study the implosion of mockups of nuclear weapons in which

the actinides have been replaced by non-fissile metals. These large-scale implosion experiments are often called "hydrotests" for short.

Point-projection radiography is the most common technique used to image these dynamic experiments. A pulsed "point" source of penetrating bremsstrahlung photons illuminates the object from behind, projecting a "snapshot" of the hydrodynamic effects onto a large area film or camera-based imaging system. Improvement of the quality of these images has motivated the direction that accelerator development has taken. Image quality is generally thought of in terms of contrast and resolution, and accelerator parameters have both direst and indirect influence on these.

Stopping the action to minimize hydrodynamic-motion blur contribution to spatial resolution sets the maximum permissible pulse-width of the accelerated electron beam. Shock pressures in high-explosive driven hydrodynamic experiments are multi-megabar, and corresponding shock velocities exceed 1 cm/μs, so the bremsstrahlung radiation pulse must be 100 ns or less to achieve millimeter scale resolution. Therefore, the accelerator must be capable of producing radiation at a high dose rate, in order to produce sufficient dose for a high-quality image within the short pulsewidth. Bremsstrahlung dose rate is roughly proportional to $IE^{2.7}$, where $I$ is the beam current and $E$ is the beam energy, thus motivating high-current, high-energy designs.

Radiation scattered by the object causes a noise background on the image, and cannot be ignored because it degrades the contrast. Scattering increases rapidly with the number of mean free paths through the object, and thus establishes an upper limit on the energy of the accelerator for acceptable contrast. Therefore, accelerator design cannot take full advantage of the strong scaling of dose with beam energy if the degradation of contrast from scatter background is fully considered.

Moreover, the useful dose for imaging is a complex folding of the bremsstrahlung spectrum, the cross-sections of the object materials, and the imaging detector sensitivity. Over the past 40 years or so, detailed experimental, analytical, and Monte-Carlo analyses of all these considerations and trade-offs have settled in on multi-kiloampere accelerator designs with energies from 10-30 MeV for hydrotests and somewhat lower energies for smaller-scale experiments. A singular exception to this is the family of 65 – 70 MeV pulsed betatrons at the All-Russian Institute of Experimental Physics (VNIIEF) in Sarov, Russia.

Resolution is ultimately limited by the radiation-source spot size, which is significantly affected by accelerator design. The spot size is determined by many factors. Taking a linear induction linac (LIA) as an example, these factors include final-focus magnet focal length, beam emittance, energy variation during the pulse, and gross beam motion during the pulse. The final-focus length is usually given as a constraint to the accelerator designer, so the emphasis has been on beam stability, with minimal motion and emittance. In an LIA the major contributors to beam motion are the beam-breakup instability (BBU) and beam "corkscrew" motion. BBU is the result of $TM_{110}$ cavity modes, and corkscrew is the result of energy variation of the beam interacting with random chromatic aberrations in the transport magnetic field. Energy stability during the pulse is important, because it affects spot size through the direct proportionality of final-focal strength with energy, as well as the dependence of corkscrew motion amplitude on energy variation.

Radiographic spot size is measured at the different laboratories in a variety of ways including pinhole cameras, "cylindrical" collimators, and "knife edges" (also called "roll-bars"), so it can be difficult to compare data from different accelerators. Moreover, there seem to be at least as many ways to report the results as there are techniques for

getting the data. As usual, the use of a single number, "spot size", does not tell the whole story, and details of the intensity distribution must be carefully considered [1]. For this review, we will try to stick to a single definition based on the modulation transfer function (MTF); the 50%MTF spot size. The 50%MTF spot size is the diameter of a uniformly illuminated disk with the same half-width MTF as the measured intensity distribution. This is the spot-size measure that has been adopted for use by Los Alamos radiographers. A useful rule of thumb for comparison is that, for a Gaussian intensity distribution, the 50%MTF spot size is ~1.6 times the full-width at half maximum (FWHM).

Dose is also measured by a variety of methods including calorimetry, TLDs, and Compton diodes. One must be even more cautious in comparing dose measurements by the different laboratories, because generally these methods are not as well cross-calibrated as the spot-size measurements. The standard means for quantifying dose is to quote the total dose on centerline at one meter from the converter.

In addition to these fundamental requirements for high-quality radiographs is the need for more information from a single hydrodynamic experiments. Especially the larger of these experiments, the hydrotests, are expensive propositions, and infrequently repeated, so there is a strong motivation for a large data return from each shot. Moreover, more than one view is necessary to resolve 3-D features. Finally, shot-to-shot timing reproducibility is problematic, motivating multiple pulses on a single shot to resolve time evolution of the features of interest. Of course, the pen-ultimate goal is 3-D radiographic cinematography.

## II. RF ACCELERATORS

The benchmark for large radiography accelerators is PHERMEX (Pulsed High-Energy Radiographic Machine Emitting X-rays) [2]. PHERMEX is a 3-cavity, 50 MHz RF standing-wave accelerator. The accelerating $TM_{010}$ mode RF power in each cavity is 2-3 MW. It was originally powered by nine RCA A-15041 beam-triode broadcast tubes, arranged so that four tubes drove the first cavity, three drove the second, and two the third. Over the years the PHERMEX RF amplifier chains were upgraded and now use eight EIMAC 8974 power tetrodes, with only three tubes driving the first cavity.

In single-pulse mode a 200-ns, 1-kA beam produced by a dispenser cathode is injected into the first cavity, where most of it is lost. About 175 A average current is accelerated to ~30 MeV as a train of ten 3.3-ns FWHM micro-pulses with 20-ns inter-pulse separation (the RF period) [3]. Figure 1 shows a representative PHERMEX micro-pulse train. This pulsetrain contains ~35-mC of charge that is focused through a Be vacuum window and short (~10 cm) air cell onto the Ta bremsstrahlung converter to produce over 400 Rad@1m.

In the late 1990s a double-pulse upgrade to PHERMEX was completed. Now it is possible to get PHERMEX radiographs with a single 60-ns, 100-ns, or 200-ns pulse, or with two 60-ns pulses separated by up to 1-ms. Each 60-ns pulse produces more than 100 Rad@1m. The radiographic spot size is less than 3-mm 50%MTF. Figure 2 shows radiographs of a test of a VIPER shaped charge using the double-pulse capability of PHERMEX.

## III. PULSELINE DRIVEN DIODES

In the UK, at the Atomic Weapons Establishment (AWE), development of single pulseline driven diode accelerators for radiography (initiated by J. C. "Charlie" Martin)

continues. This has proven to be a very cost-effective approach, with the result that AWE now has a multitude of accelerators available, with no less than five of their high-explosive containment chambers capable of providing two views. The present complement of AWE accelerators is summarized in Table I. Figure 3 is an artist's rendition of the largest AWE hydrotest facility, which uses Mogul D and Mogul E to provide two views at 140°.

All of the AWE machines have a Marx-generator charged oil-insulated Blumlein pulse-forming line as the pulsed-power driver for the diode. In the Moguls and Superswarfs the pulse-forming line is switched into a magnetically insulated transmission line (MITL) that drives a gas-focused paraxial diode. The Mevex' and Mini Bs use pinched diodes or rod-pinch diodes, which will be described later.
The high-current AWE accelerators provide an interesting counterpoint to PHERMEX, which depends on the beam energy to provide the required dose at much lower current. The difficulty with the high-current approach presently appears to be in obtaining a small spot size from the high-current diodes, but progress continues to be made in that arena.

AWE is now designing a new hydrodynamic experimental facility with up to five accelerators for five independent views. They are presently working with Sandia on designs using compact, modular inductive voltage-adder (IVA) technology, enabling even higher-energy (14-MeV) high-current accelerators.

## IV. INDUCTIVE-VOLTAGE-ADDER DRIVEN ROD-PINCH DIODES

Most modern developments in radiography have been evolutionary, but two break with tradition, and might be called revolutionary. These are the use of inductive voltage adder (IVA) technology and the rod pinch diode.

Sandia has been developing IVAs for high-voltage, pulsed-power applications since the Helia technology demonstration project in 1984. A schematic diagram of single IVA cavity is shown in Fig.4. A high voltage pulse is applied to the gap by an external pulse-power generator. The high voltage side of the gap is inductively isolated from ground by the toroidal inductor for a time determined by the flux swing of the core (volt-seconds) and the applied voltage. Several cells are connected in series to form the IVA, which has an output voltage equal to the sum of the individual drive voltages. The center conductor is usually tapered or stepped down at each cell so that the impedance of the structure is approximately constant as a function of length, even though the voltage increases at each gap.

One obvious application of the IVA is to raise the voltage of high-current diode radiography machines such as those at AWE. Another application is for a class of compact radiography accelerators for small-scale hydrodynamic experiments where space is at a premium, e.g. the underground sub-critical experiments for the stockpile stewardship program. The modularity of the IVA architecture lends itself to compact systems that can be squeezed into the odd nook or cranny available in those tunnels.

The rod-pinch diode, developed by Naval Research Laboratory (NRL), consists of a small anode rod extending through an annular washer-like cathode. At high currents a magnetically insulated flow of electrons from the cathode to the tip of the anode results in a very small radiographic spot. An aggressive experimental campaign to develop this device as a radiographic source has been carried out at NRL, Bechtel Nevada (BN), Sandia National Laboratories, and Centre D'etudes de Grammat (CEG) in France. The accelerators used in these experiments include the 1.1-MeV, 35-kA TriMev at BN; the 2.3-MeV, 60-kA Sabre IVA at Sandia; the 4-MeV, 100-kA ASTERIX at CEG; and the 2-MeV, 1-MA Gamble-II at NRL.

The scaling of the rod-pinch radiographic performance with energy is a remaining issue, if it is to be applied in hydrotest experiments needing a higher-energy, penetrating spectrum. In any case, for the moderate energies from 1-5 MeV required for smaller-scale hydrodynamic experiments the rod-pinch diode is a significant advance for radiography.

Using an IVA accelerator to drive a rod-pinch diode would seem to be an ideal marriage of technologies. In one such effort Sandia and Los Alamos are teaming to develop the CYGNUS IVA accelerators for two views of experiments in a sealed explosion chamber. Each accelerator will use a single Marx powered pulse line connected to three IVA cavities in parallel with a 30□ output MITL to the diode. To meet the aggressive schedule for fielding the completed CYGNUS machine Sandia is "mining" the Sabre accelerator for the induction cells that will be used in CYGNUS, using an existing Sandia design for the pulse forming line, and purchasing commercially available Marx generators.

The 2.2 MV CYGNUS output pulse will drive a rod-pinch diode predicted to have a 50%MTF spot size less than 0.8 mm and produce a dose of about 10 Rad@1m. As part of this project, rod-pinch diode tests on the 2.3-MeV, 60-kA SABRE IVA accelerator at Sandia have already demonstrated an 0.8-mm 50%MTF spot size with a dose of 3 Rad@1m.

## V. PULSED BETATRONS

A unique approach to the problem of radiographing hydrodynamic experiments has been taken by VNIIEF, where they have pursued development of the air-core pulsed betatron invented by A. I. Pavlovskii [4]. The newest of these are all based on an

accelerating tube design having an equilibrium beam orbit radius of 234 mm, hence their descriptive nomenclature: BIM-234. These betatrons all accelerate the beam to energy of 65-70 MeV. The radiation output is obtained by using a fast magnetic field to quickly change the orbit, pushing the beam into a converter target located inside of the toroidal vacuum tube. The various BIM accelerators differ from each other mainly in details of the beam injectors and the fast pulse output windings.

There are several small BIM-234 series accelerators at different VNIIEF high-explosive sites, most with output dose in the 2-5 Rad@1m range. Some of these have been modified to produce up to three output pulse, usually 100-500 ns wide over a period of ~2 μs. At least one site has two of the small machines at 90° for dual view radiographs of small hydrodynamic experiments.

The newest and largest betatron at VNIIEF is BIM-M [5]. Figure 5 is an outline drawing of this compact device, which fits into a volume of about 7 m X 3 m X 3 m, exclusive of the main betatron capacitor bank. The BIM-M injector is a cold-cathode diode driven by a Marx/pulseline/MITL. This produces a 2-MeV, 10-kA, 15-ns electron beam. About 500 A is actually injected into the ring, and about 280 A is trapped in the magnetic well as circulating current. A 400-kJ capacitor bank is discharged into the 50-μH betatron magnet winding to accelerate the beam from the 2-MeV injection energy up to the 50-70 MeV final energy in 550 μs.

As with all of the VNIIEF betatrons, the BIM-M radiation spot is elliptical; ~3.2 x 8.0 mm 50%MTF. The maximum dose in a single pulse is 100-150 Rad@1m. BIM-M also has three-pulse radiographic capability. Figure 6 shows the radiation intensity from three BIM-M pulses.

## VI. LINEAR INDUCTION ACCELERATORS

The modern ships-of-the-line for hydrotest radiography are three linear induction accelerators (LIAs) presently in operation in the US and France. (The LIA can be thought of as simply an IVA in which center conductor is replaced by an electron beam). The parameters of the three operational radiography LIAs are summarized in Table 2. These accelerators bear a close resemblance to each other (e.g. all use ferrite-cored induction cells and cold-cathode injectors), but differ significantly in design details.

### *A. FXR*

FXR at Livermore was the first linear induction accelerator designed specifically for hydrotest radiography (Fig. 7). It began operations in 1982 with beam parameters of 2.2 kA at 17 MeV. It uses 44 ferrite-loaded induction cells with 300-350 kV accelerating potential per cell. Focusing solenoids on each cell with spacing close enough to provide a continuous field to suppress BBU growth provides beam transport.

FXR underwent a performance upgrade between 1991 and 1996 [6]. The original injector was replaced by one. using ten induction cells to drive the cathode. The new injector produces a higher energy (2.5 MeV vs. 1.2 MeV), higher current (2.3-3.4 kA vs. 2.2 kA) beam.

The upgrade also entailed replacing 62 focusing solenoids. Unlike the originals, the new magnets have bifilar windings and homogenizing rings to minimize field errors, and incorporate printed-circuit steering dipoles. Much attention was paid to accurate alignment of the magnets when they were installed, because the beam corkscrew motion at the accelerator exit is essentially the result of random chromatic aberrations due to misalignment and small field errors.

Mode damping ferrites were also added to the accelerating cavities during the upgrade to reduce the BBU instability, and beam position monitors were installed at 16 locations down the beam line.

A new tuning algorithm to minimize beam corkscrew motion was implemented that took full advantage of the improved capability to measure and control beam position. As a result of the upgrade the FXR parameters were significantly improved to those shown in Table 2.

### *B. DARHT-I*

DARHT-I is the accelerator recently completed for the first of two orthogonal views for the Los Alamos Dual-Axis Radiographic Hydrodynamic Testing facility (Fig. 8). The DARHT-I accelerator became fully operational in 1999. It uses 64 ferrite-loaded induction cells to accelerate the 2.5 MeV, 1.7 kA beam injected by a cold velvet-cathode diode driven by a single pulseline. The cell accelerating potential in DARHT-I is somewhat lower than that of FXR; 275 kV compared with more than 300 kV.

The DARHT-1 focusing-solenoid design took advantage of the FXR experience and includes both homogenizing rings and steering dipoles. Moreover, a pulsed-wire wire technique was used to accurately locate each magnet centerline and relate it to external fiducials for accurate optical alignment when the accelerator was assembled. A significant effort was made to minimize the variation of energy throughout the flat top portion of the DARHT-I pulse as a further attack on the chromatic corkscrew motion. As a result, the initial corkscrew amplitude was small enough that it was possible to use a much simpler tuning algorithm than that used on FXR.

The result of all of this attention to detail was a reduction of combined corkscrew and BBU motion at the accelerator exit of ± 0.5 mm, or about 3% of the beam radius, and thus a very small contribution to spot size.

DARHT-I was well instrumented at the outset with more than 20 beam position monitors. These differ from the FXR position monitors in that they use B-dot loops to locate the beam through the magnetic fields it produces, rather than the wall return current as in the FXR resistive wall monitors.

At the accelerator exit there is provision for a variety of beam diagnostics, including a magnetic spectrometer with streak camera read out, optical transition radiation measurements of beam current density profile and emittance, and diamagnetic loop measurements of beam size. These have been used to provide a detailed characterization of the beam. Using these diagnostics the beam energy variation throughout the flat top has been measured to be less than ± 0.5%.

With its 2-mm 50%MTF spot size and over 500 Rad@1m bremsstrahlung pulse DARHT-I has provided some of the best quality radiographs of hydrotests ever, and it has a full dance card of hydrotests planned for the next several years.

### *C. Airix*

Airix, the newest of the operational LIAs, was built at the PEM facility at Moronvilliers, France for radiography of hydrotests. Like DARHT-I, Airix uses 64 ferrite-loaded cells to accelerate the beam injected by a single pulseline driven cold-cathode diode. A major difference between Airix and DARHT is that the entire acceleration cell, including the ferrite cores, is under vacuum with an air-vacuum interface at the drive-rod feedthroughs. This eliminates the need for an oil-vacuum interface. Another innovation on Airix is the use of a hydraulic system to align the accelerator magnetic axis, in

addition to the use of the pulsed-wire technique. This resulted in an order of magnitude improvement of the accelerator alignment.

As on DARHT, a significant amount of work went into minimizing the energy variation during the flat top of the pulse. At 19.2 MeV the energy variation is ±0.3% over 60 ns (Fig. 9). The net result of all this is that the Airix beam motion is less than 2% of the beam radius at the accelerator exit. All of this attention to detail has paid off in spot size. At 1.8 mm, Airix has the smallest spot size of the three operational radiography LIAs.

### *D. DARHT-II*

The accelerator for the second axis of DARHT is presently being installed, and is expected to become operational in 2003. DARHT-II is being built as a collaborative effort between Los Alamos, Livermore, and Berkeley National Laboratories. It will produce an 18.4-MeV, 2-kA, 2-μs beam that will be sliced into four pulses of about 100 ns or less each by a fast kicker system at the accelerator exit. This will provide four radiographs with a view orthogonal to the single DARHT-I radiograph, as shown in Fig. 8. Figure 10 is a layout of the DARHT-II accelerator showing the major components.

The injector for DARHT-II (Fig. 11) is powered by a Marx generator consisting of 88 type E PFNs. This produces a flat 2-μs 3.2-MV output pulse with a 400-ns risetime into a matched load. However, because of the stray capacitance of the 4.44-m insulating column, the actual risetime at the diode will be over 500 ns.

The oil-filled vertical insulating column is a bonded structure of mycalex and ceramic rings interspersed with metal grading rings that are internally connected by strings of resistors and MOVs. A 16.5-cm diameter hot dispenser cathode in a

shrouded Pierce-like diode will produce the beam. Eight large-bore (36-cm diameter beam tube) 173-kV induction cells will then further accelerate the beam to 4,6 MeV.

After these first eight cells the beam enters a special beam-head cleanup zone (BCUZ) with a very narrow energy bandpass to scrape off the long risetime beam head. Then the beam enters the main accelerator, which. consists of 70 smaller-bore (25.4-cm diameter beam tube) 195-kV induction cells.

DARHT-II is heavily instrumented with beam diagnostics. There are 30 beam position monitors: three in the anode region, three in the BCUZ, one at the entrance to each block of six cells, and 13 in the downstream transport/kicker/target region. The accelerator monitors incorporate new optically-isolated electro-optic capacitive detectors to provide accurate low-frequency beam position data even if there are electrical ground-loops present. (Ground loops have not been a problem with the present 60-ns pulse LIAs, because everything – pulsed power and diagnostics alike – is transit-time isolated; not so on the 2-μs DARHT-II). The position monitors also have B-dot detectors for measuring the high-frequency motion due to BBU. The BBU frequency is beyond the bandwidth limitation of the electro-optic detectors, and low-frequency ground-loop backgrounds can be readily filtered out of these signals. Diamagnetic loops for measuring the beam size are located at each of the 12 beam position monitors in the main DARHT-II accelerator, and two more loops are strategically positioned in the downstream transport. This will be the first LIA to have non-invasive diamagnetic beam size measurements as an integral component of the online diagnostics package for accelerator tuning.

## VII. CONCLUSIONS

There have been significant improvements in capability for obtaining high-quality radiographic data from hydrodynamic experiments over the past few years.

Radiography of smaller-scale hydrodynamic experiments has advanced as a result of the application of IVA technology and the invention of the rod-pinch diode. Large-scale hydrotest radiography has progressed as a result of continuous improvements of large linear-induction accelerators, which produce high-quality, stable electron beams. These LIAs have achieved spot sizes less than 2 mm (50%MTF), with doses up to 650 Rad@1m. With the advent of the DARHT-II accelerator in a few years we will have available a hydrodynamic test facility with radiation pulses in that parameter range for two orthogonal views, with four pulses from one of them.

Finally, as shown in Table 3, our first full-energy beam experiments with DARHT-II in 2003 will mark 40 years of continuous improvement of Nick Christofilos' concept for accelerating high-current electron beams [8]. Beginning with Christofilos' original use as the electron injector for forming the e-layer in the ASTRON controlled fusion device the LIA has been found many uses, including weapon effects and endo-atmospheric propagation. Most recently, the LIA has become the leading accelerator technology for hydrotest radiography at the US and French nuclear weapon laboratories.

## VIII. ACKNOWLEDGEMENTS

The author is deeply indebted to the following individuals and laboratories for their generous contributions to this review: Tim Goldsack, Ray Edwards (AWE); John

Maenchen (Sandia); Gerry Cooperstein (NRL); Yuri Kuropatkin (VNIIEF); Eric Merle (CEA/PEM); Ray Scarpetti, John Weir (Livermore); Dave Moir, Christophe Vermare, Scott Watson, Alan Wadlinger, Doug Fulton, and Randy Carlson (Los Alamos). Without their help, this review would not have been possible.

This research was supported by US Department of Energy contract W-7405-ENG-36 with the University of California.

## IX. REFERENCES

[1] K. Mueller, "Measurement and Characterization of X-Ray SpotSize," in Proceedings of the Flash Radiology Topical, American Defense Preparedness Assoc., 1989, pp.383-394.

[2] Douglas Venable, Editor, "PHERMEX: A pulsed high-energy radiographic machine emitting x-rays," Los Alamos National Laboratory Report, LA-3241, May, 1967

[3] Thomas P. Starke, "PHERMEX standing-wave linear electron accelerator," presented at the 7th Conference on the Application of Accelerators in Research and Industry, Denton, TX, 1982

[4] A. I. Pavlovskii, G. D. Kuleshov, G. V. Sklizkov, Yu. I. Zysin, and A. I. Gerasimov, "High-current ironless betatrons," Soviet Physics Doklady, vol. 10, (no. 1), pp.30-32, July, 1965

[5] Yu. P. Kuropatkin, V. D. Mironenko, V. N. Surorov, D. I. Zenkov, and B. F. Tkachenko, "Uncored betatron BIM-M a source of bremsstrahlung for flash radiography," in Proc. 11th IEEE Int. Pulsed Power Conf., 1997, pp. 1669-1673

[6] R. D. Scarpetti, N. L. Back, J. K. Boyd, G. G. Earley, K. L. Griffin, R. G. Kerr, R. Kihara, M. M. Ong, and J.-M. Zentler, "Upgrades to the LLNL flash x-ray induction linear accelerator (FXR)," in Proc. 11th IEEE Int. Pulsed Power Conf., 1997, pp.597-602

[7] E. Merle, J. Bardy, R. Boivinet, F. Bombardier, A. Devin, M. Mouillet, O. Pierret, and J. C. Ribes, "Transport of the 2 – 3.1 kA AIRIX electron beam," Proc. Part. Acc. Conf., 2001, to be published

[8] N. C. Christophilos, R. A. Hester, W. A. S. Lamb, D. D. Reagan, W. A. Sherwood, and R. E. Wright, "High current induction accelerator for electrons," Rev. Sci. Instrum., vol. 35, pp. 836-890

TABLES AND FIGURES

Figure 11. Artist rendition of the injector for the DARHT-II accelerator.

| *Accelerator* | *Energy (MeV)* | *Current (kA)* | *Pulse (ns)* | *Spot Size 50%MTF (mm)* | *Dose Rad@1m* |
|---|---|---|---|---|---|
| Mogul E | 10 | 35 | 80 | ~5.5 | 600 |
| Mogul D | 7 | 30 | 80 | ~4.9 | 220 |
| Superswarf | 5.5 | 30 | 60 | ~4.9 | 80 |
| Mini B | 2.2 | 30 | 50 | ~3.3 | 12 |
| Mevex | 0.8 | 35 | 50 | ~2.7 | 1.2 |

Table 1. Single Pulseline diode accelerators at AWE

| *Accelerator* | *Laboratory* | *Energy (MeV)* | *Current (kA)* | *Pulse (ns)* | *Spot-Size 50%MTF (mm)* | *Dose Rad@1m* |
|---|---|---|---|---|---|---|
| FXR | LLNL (US) | 18 | 2.3–3.4 | 65 | 3.2–3.5 | 325–400 |
| DARHT-I | LANL (US) | 20.0 | 1.7 | 60 | 1.9–2.1 | 550–650 |
| AIRIX | PEM (FR) | 19.2 | 1.9–3.1 | 60 | 1.6–2.0 | 350 |

Table 2. Operational linear-induction accelerators for radiography.

| *Accelerator* | *Laboratory* | *Year* | *Current (kA)* | *Energy (MeV)* | *Pulse (ns)* | *Purpose* |
|---|---|---|---|---|---|---|
| Astron-I | LLNL (US) | 1963 | 0.35 | 4 | 250 | Fusion |
| Astron-II | LLNL (US) | 1968 | 0.85 | 6 | 300 | Fusion |
| ERA | LBL (US) | 1970 | 0.9 | 4 | 60 | Fusion |
| LIU -10 | VNIIEF (RU) | 1977 | 50 | 14 | 20 | Effects |
| ETA | LLNL (US) | 1978 | 10 | 5 | 50 | Development |
| FXR | LLNL (US) | 1982 | 3 | 18 | 65 | **Radiography** |
| ETA II | LLNL (US) | 1983 | 2 | 6 | 70 | Development |
| ATA | LLNL (US) | 1984 | 10 | 45 | 80 | Propagation |
| RADLAC-II | SNLA (US) | 1985 | 20 | 20 | 20 | Propagation |
| LIU-30 | VNIIEF (RU) | 1989 | 100 | 40 | 20 | Effects |
| DARHT-I | LANL (US) | 1999 | 1.7 | 20.0 | 60 | **Radiography** |
| AIRIX | PEM (FR) | 1999 | 1.9 | 19.2 | 60 | **Radiography** |
| DARHT-II | LANL (US) | 2003 | 2 | 18.4 | 2000 | **Radiography** |

Table 3. History of linear induction accelerator development.

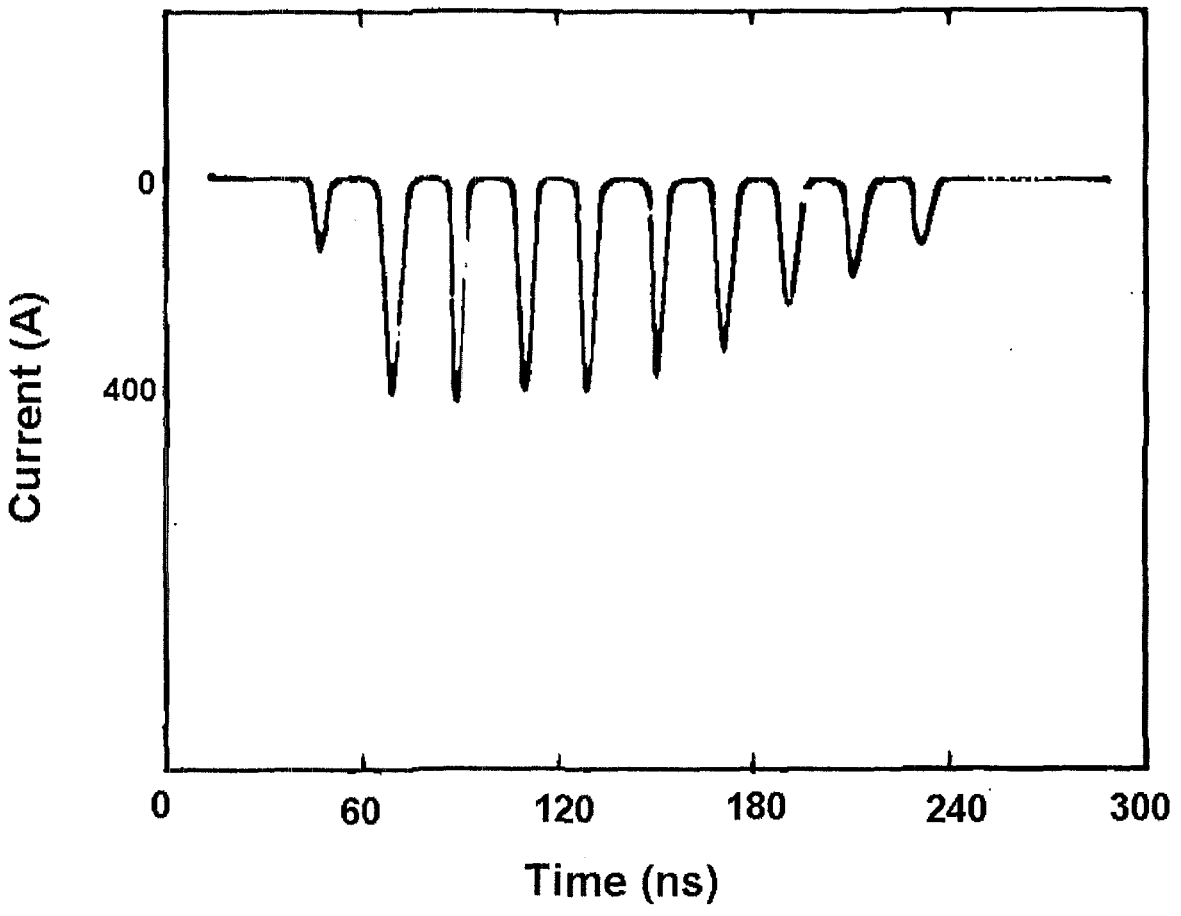


Figure 1. Phermex pulse showing RF microstructure [3]. The 3.3 ns FWHM micropulses are separated by 20 ns

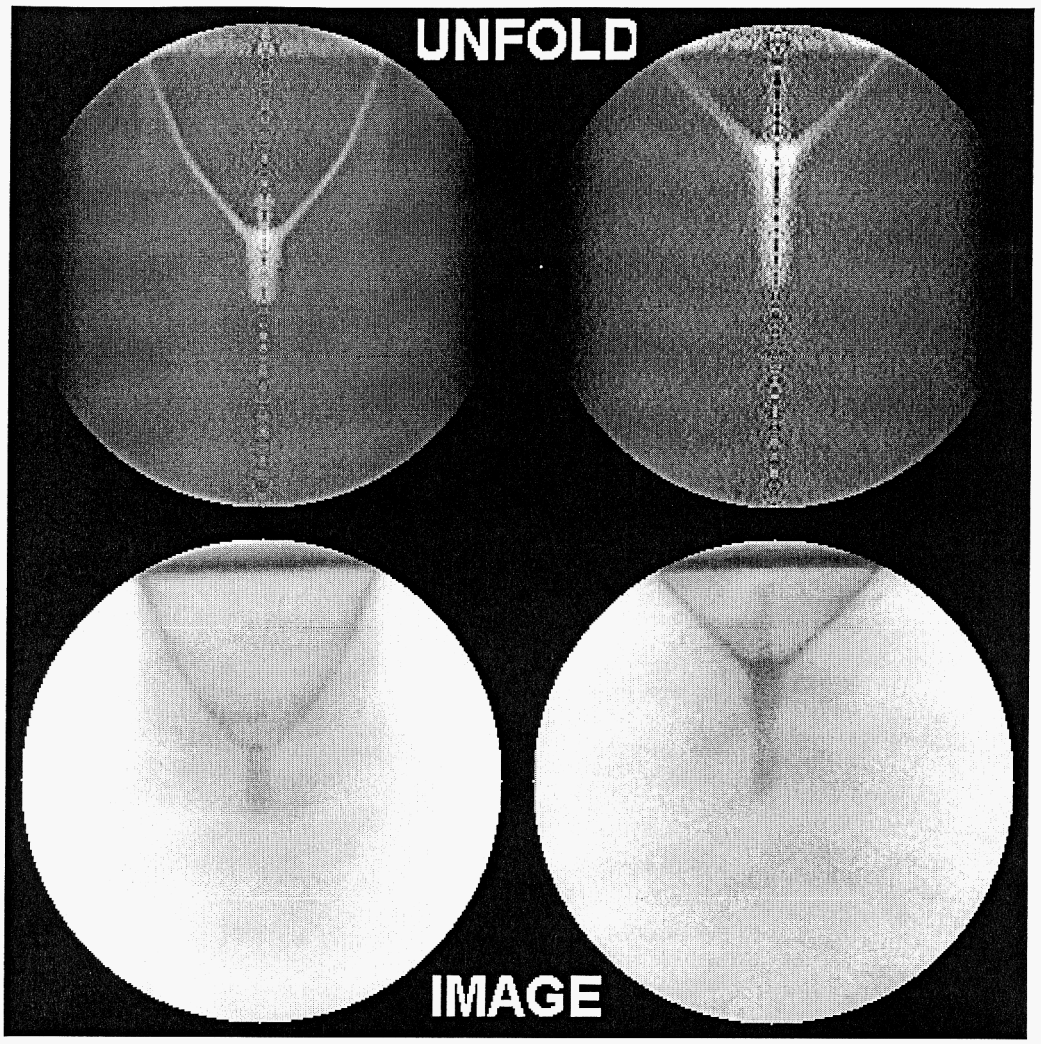


Figure 2. Double-pulse PHERMEX radiographs of Viper shaped charge. Bottom: raw images. Top: equivalent density unfold. Left: 17 μs after detonation; Right: 21 μs after detonation. The circular field of view is 15-cm diameter at the object plane.

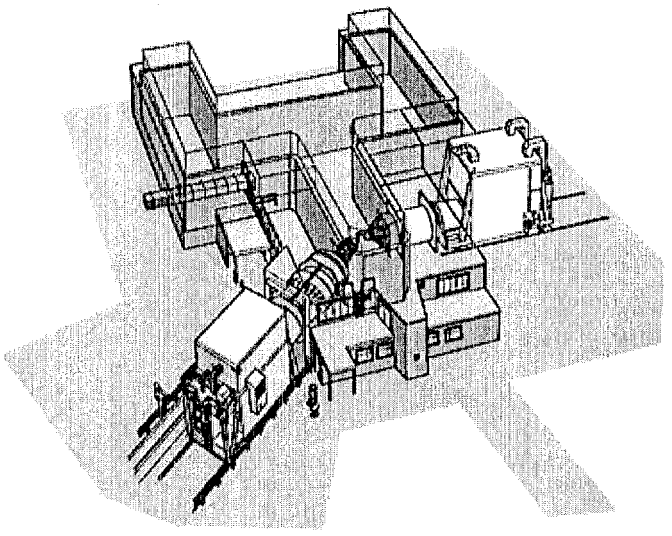

Figure 3.The AWE firing chamber that uses Mogul D (left foreground) and Mogul E for two views of hydrotests at 140°.

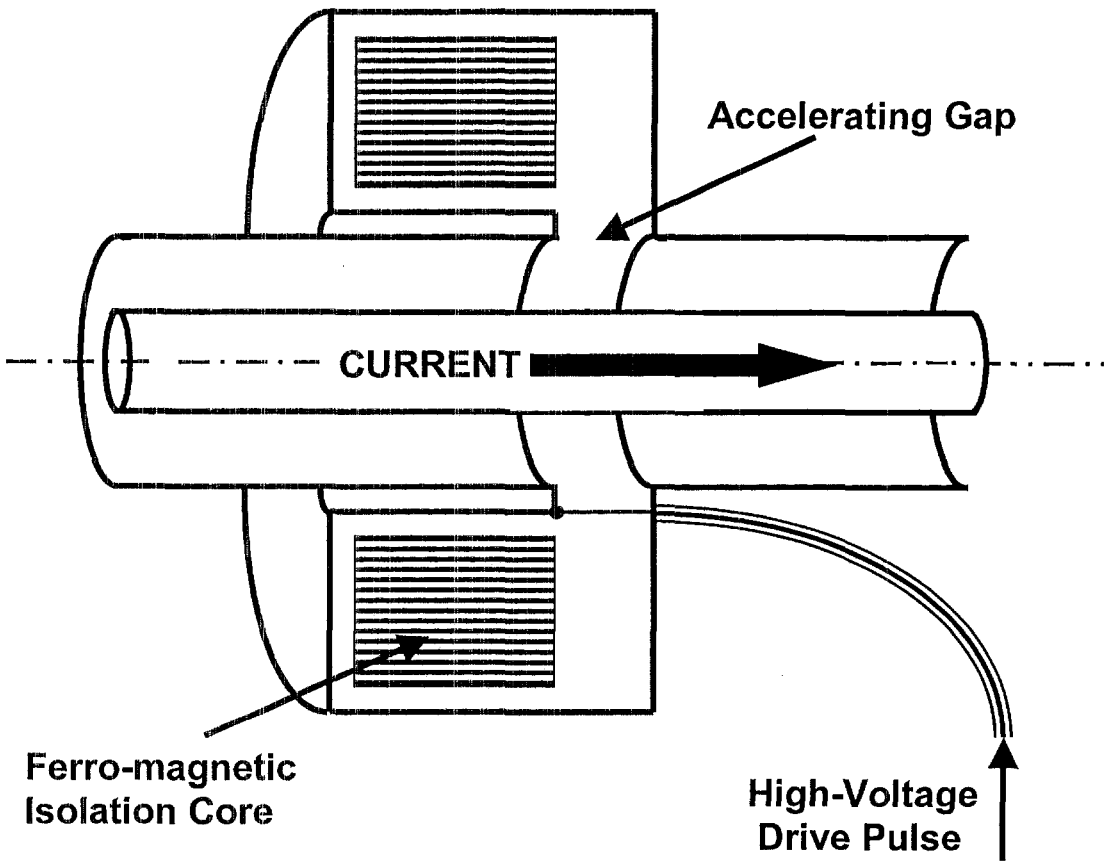


Figure 4. Inductive adder cavity.

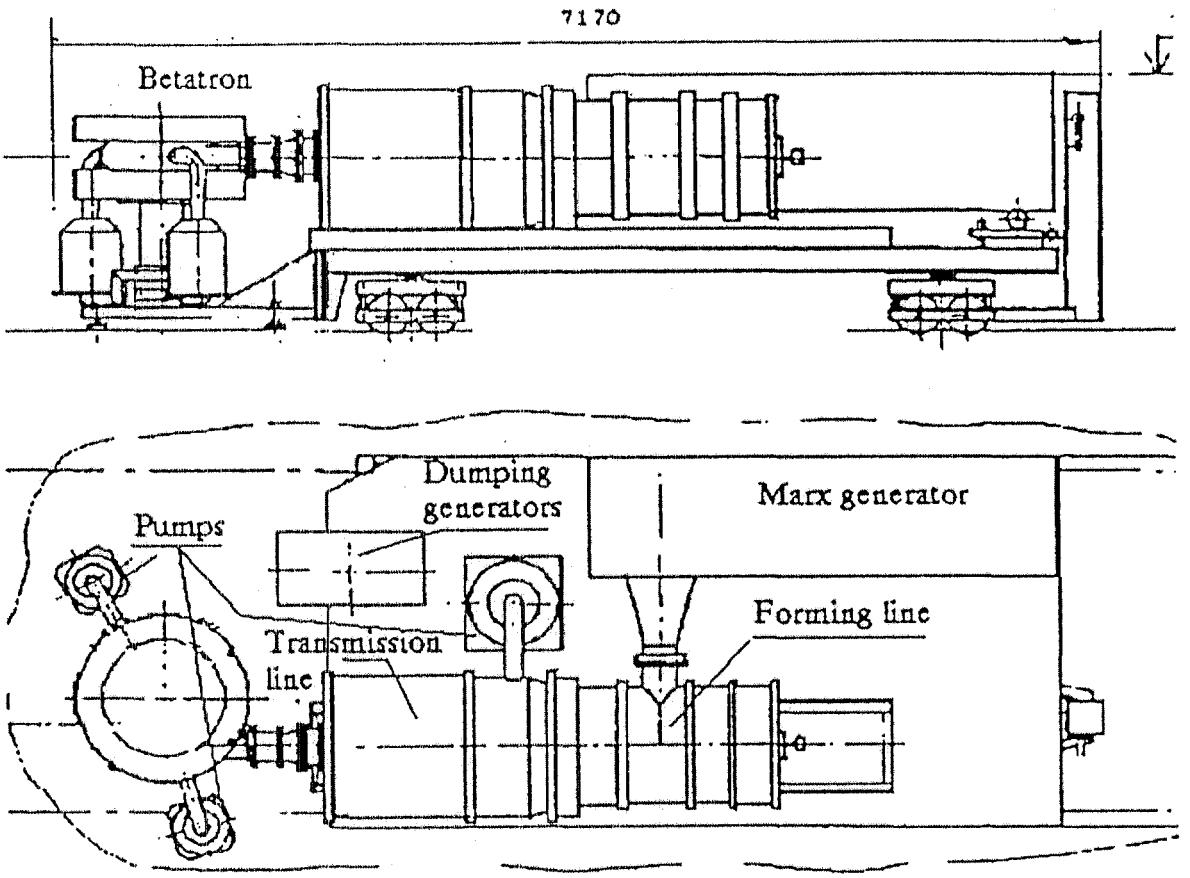


Figure 5. BIM-M betatron accelerator [4].

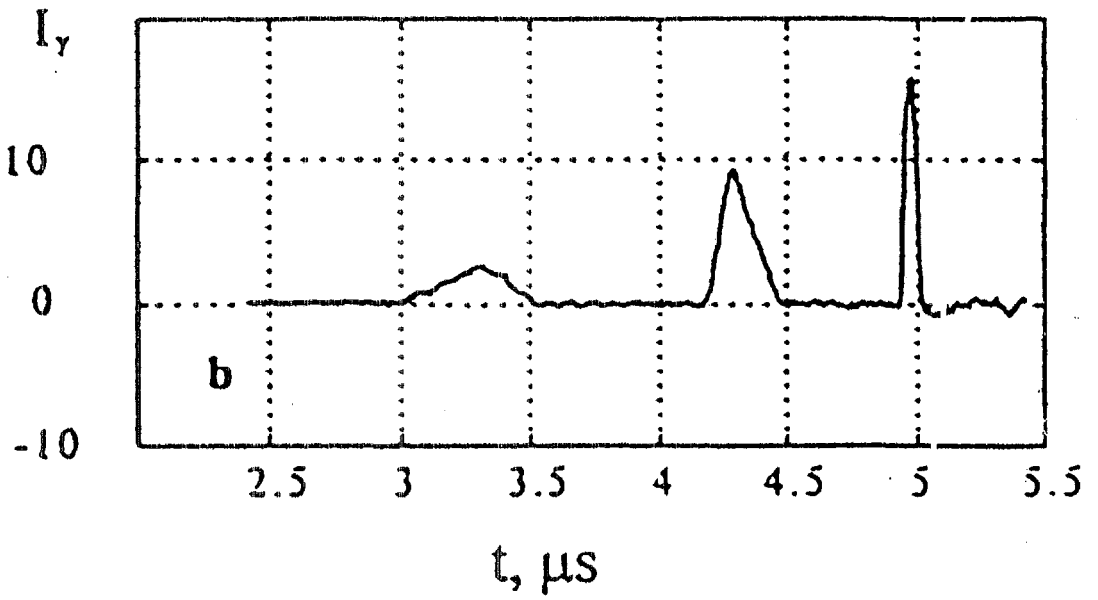


Figure 6. Three radiation pulses from the BIM-M betatron at VNIIEF [4].

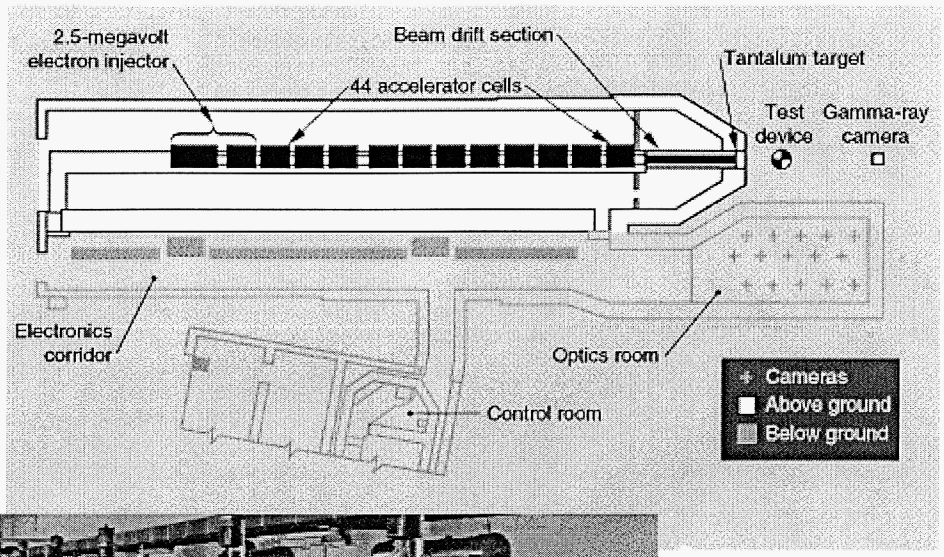


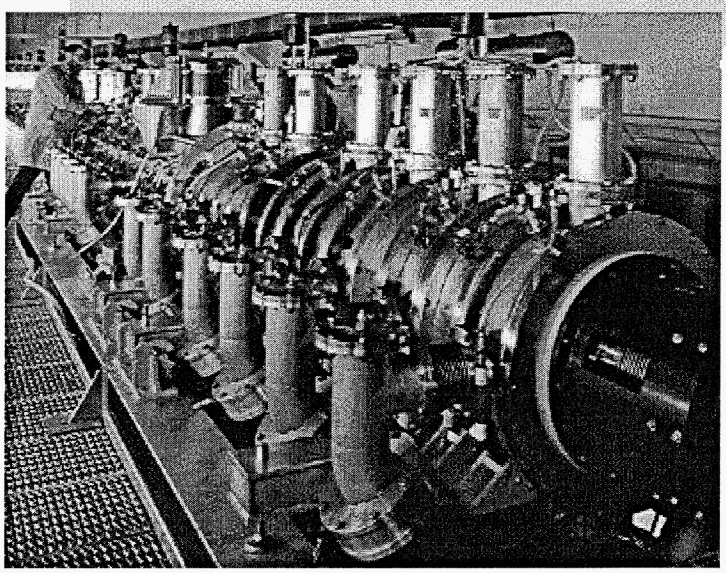

Figure 7. Livermore FXR hydrotest facility. The electronics corridor, optics room, and control room are underground, while the accelerator is on the same elevated level as the firing pad and gamma-ray imaging camera. The photograph shows several of the acceleration cells in the main accelerator hall.

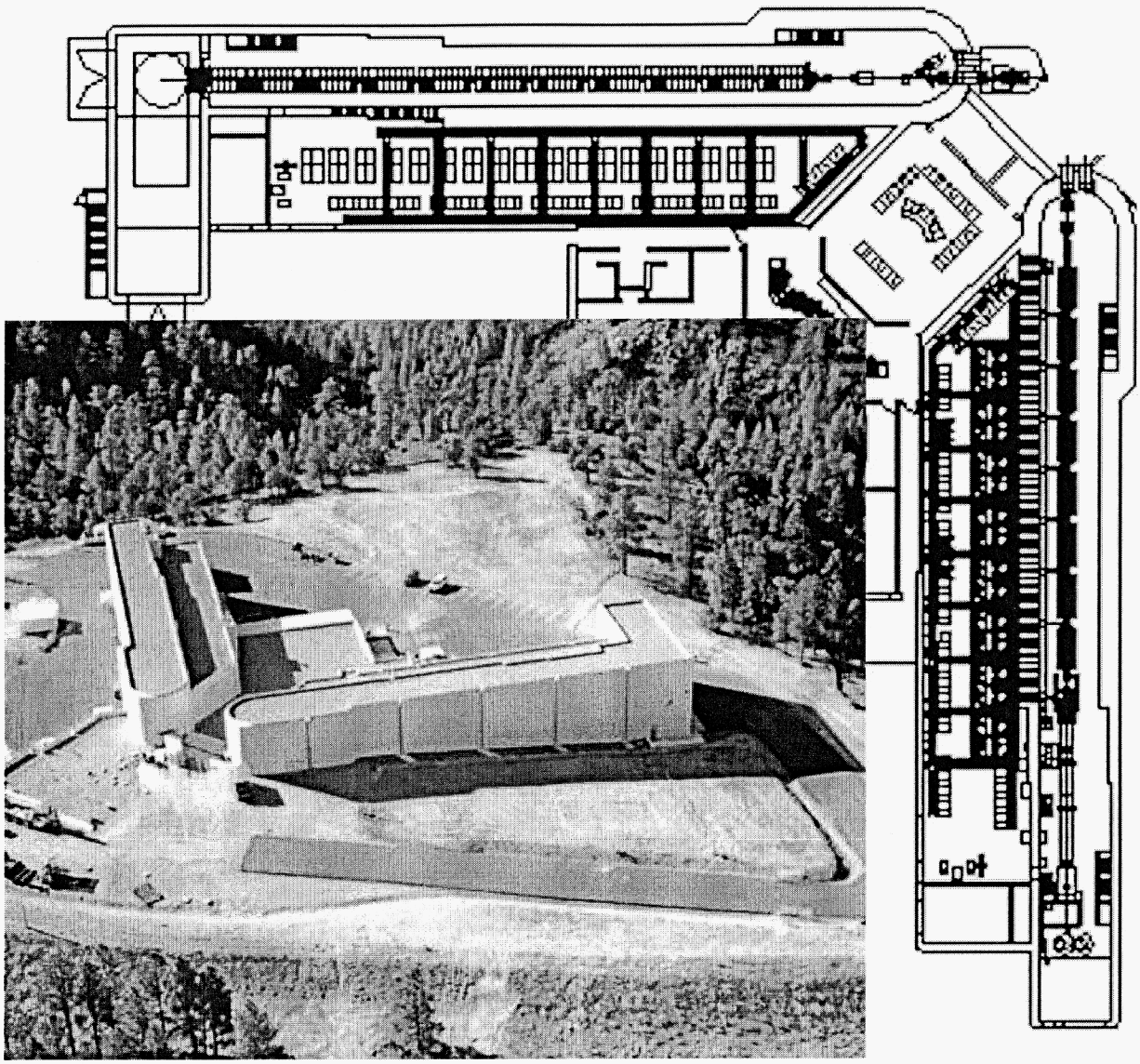

Figure 8. Aerial photograph of the Los Alamos DARHT facility overlaid on a line drawing showing the first axis accelerator (right) and the second axis accelerator (top).

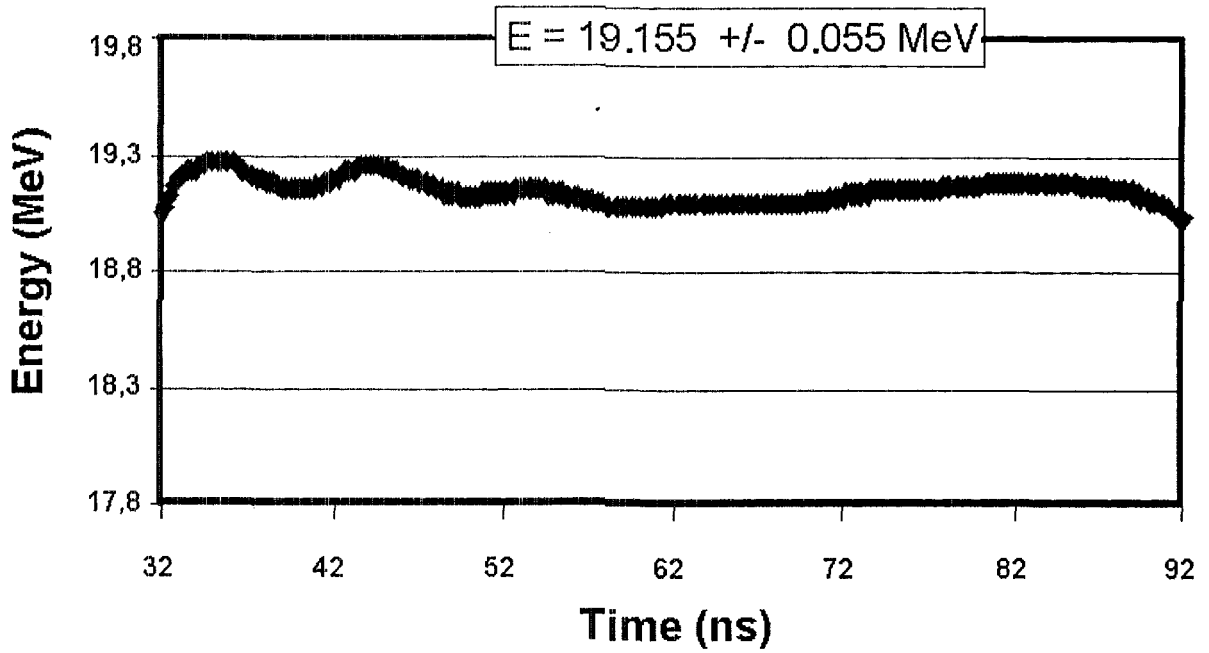


Figure 9. Airix beam energy [7]. The beam energy variation is less than 0.3% for more than 60 ns, yielding a stable final focus and minimal corkscrew.

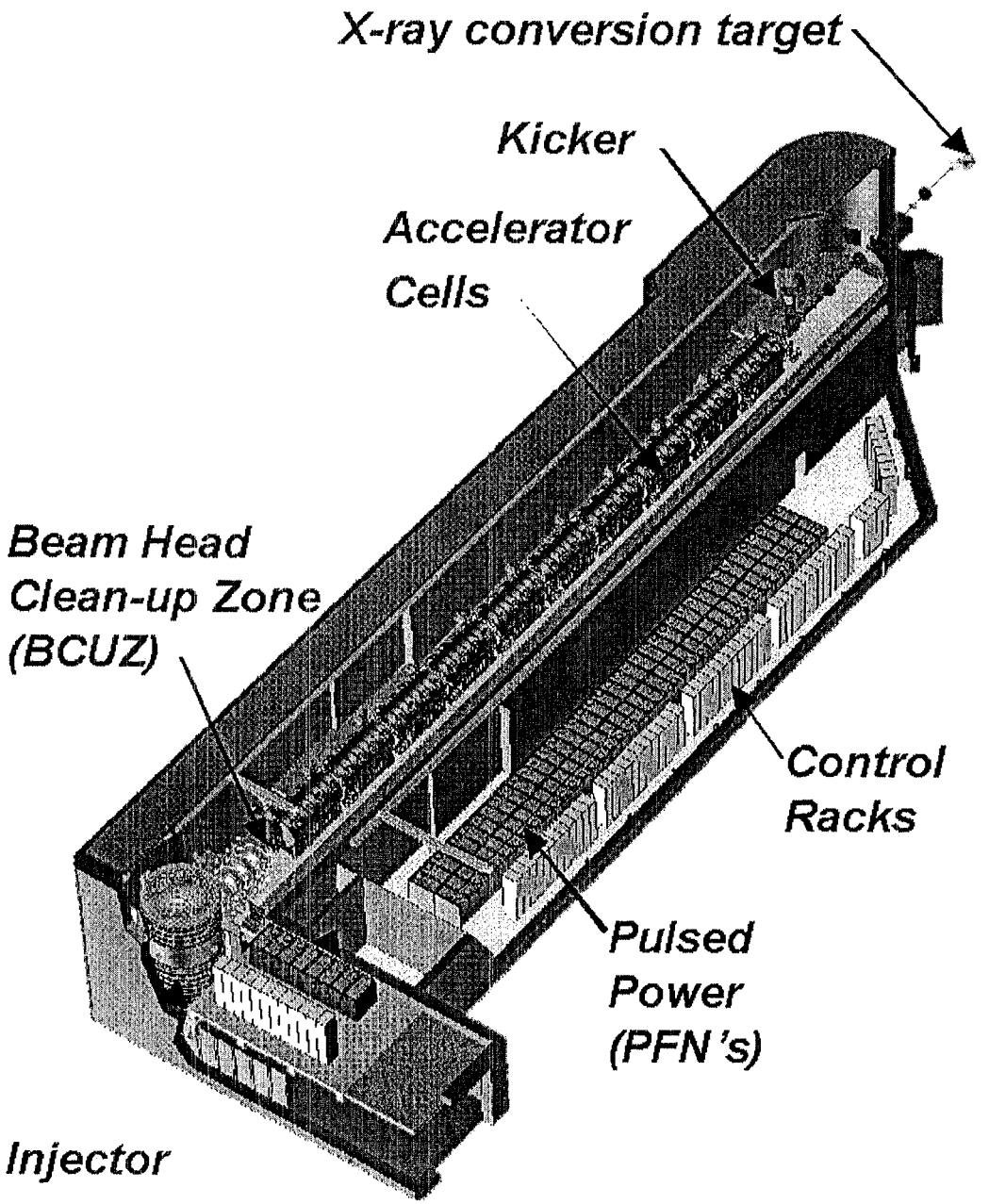


Figure 10. Layout of the DARHT-II 2-μs pulse-width accelerator.

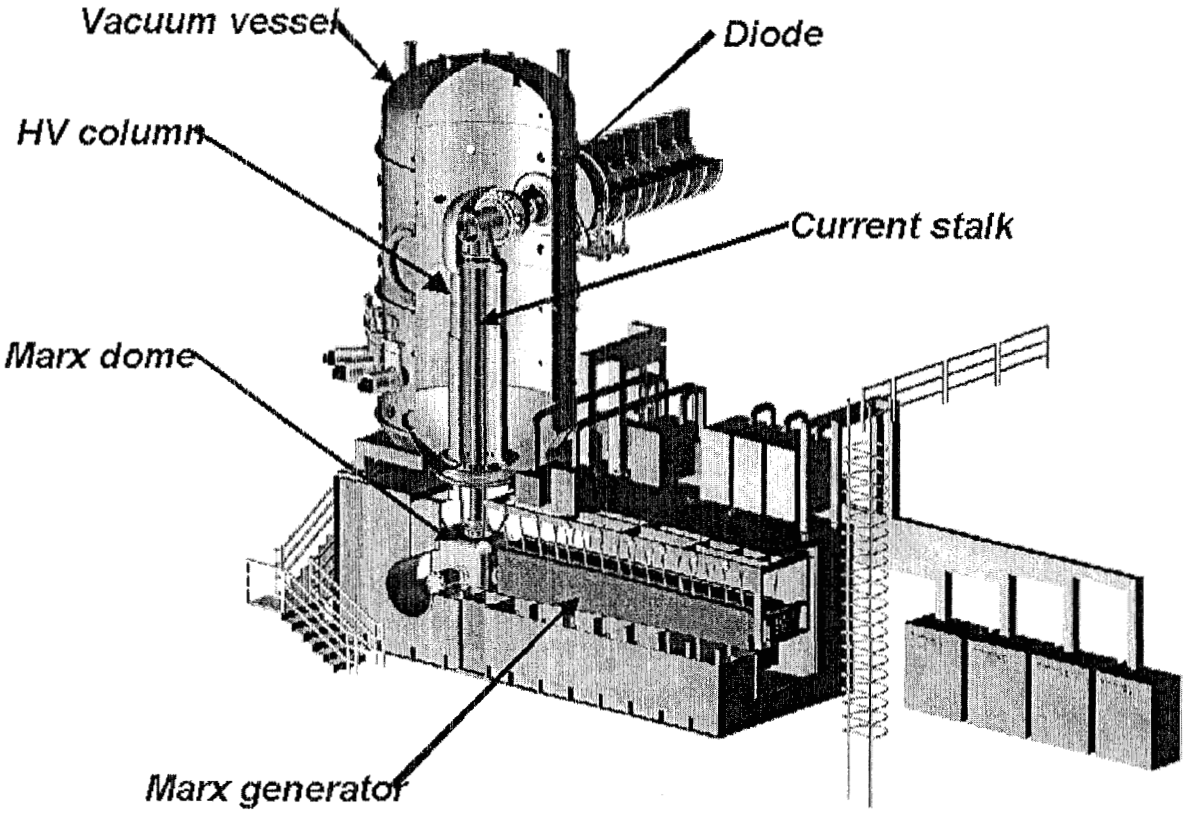


Figure 11. Artist rendition of the injector for the DARHT-II accelerator.